Heritage Science

RESEARCH

Open Access

Illuminating the problem of blue verditer synthesis in the early modern English period: chemical characterisation and mechanistic understanding

Ellen H. Purdy[1], Sarah Critchley[2], Andrea Kirkham[3] and Michael Casford[1*]

Abstract

We present a study into early modern English production of blue verditer, an early synthetic copper-based blue pigment chemically analogous to azurite. Verditers have been identified in numerous wall and easel paintings. While initial documentation occurs in the mid 1500s and production recipes were documented by the 17th c., the synthesis was known to be unreliable. This study replicates historical and recent scientific work on blue verditer and represents a significant advance in our understanding of verditer production and its challenges. Procedures for verditer synthesis are drawn from both 17th c. documentation and 20th c. replication work. The effects of temperature, copper and carbonate sources, solution stirring, copper ion concentration, and atmospheric composition are studied in order to elucidate the mechanism of synthesis and explain its unreliability in early modern refineries. Products are characterised by polarised light microscopy, scanning electron microscopy, Raman spectroscopy, and powder X-Ray diffraction. Rouaite, a green basic copper nitrate, is for the first time confirmed as a product of the refiners' synthesis and a precursor to blue verditer in laboratory syntheses. This result problematises the blanket identification of green verditer as basic copper carbonate and provides important clues to the mechanism for blue verditer synthesis. Solution chemistry and ion equilibria allow us to explain the route by which rouaite is first formed and then converted to blue verditer. Conditions favouring blue verditer production are also clarified further. Although it is commonly stated that low temperatures are required for blue verditer production, blue verditer is produced here at a range of ambient temperatures. The reaction is found instead to be controlled by solution equilibria and heavily favoured by high partial pressures of carbon dioxide. Alongside archival materials about refining and verditer production, these results are contextualised and explanations for the unreliability of historical synthesis are proposed.

Keywords Pigment production, Historical synthesis reproduction, Azurite, Verditer, Malachite, Rouaite, Wall painting

Introduction

Blue: worth its weight in gold

In the medieval and early modern periods, European painters had few choices when it came to blue pigments. Ultramarine pigment, produced from the rare mineral lazurite (a component of lapis lazuli), was difficult to source and prohibitively expensive for all but the finest work, although it produced the finest blue colour [1, 2]. Another blue mineral, azurite, produced a good pigment, but was still extremely valuable [3, 4]. The expense of

*Correspondence:
Michael Casford
mtlc2@cam.ac.uk
[1] Department of Chemistry, University of Cambridge, Lensfield Rd, Cambridge CB2 1EW, UK
[2] Cologne Institute of Conservation Sciences, Cologne University of Applied Sciences, 50678 Cologne, DE, Germany
[3] Andrea Kirkham Conservation Ltd, 31 Silver Street, Norwich NR3 4TT, UK

azurite (and ultramarine) drove painters and scientists to seek out alternative methods of obtaining blue pigments, including by synthetic routes.

Blue and green verditers are synthetic copper-containing pigments. Blue verditer is a copper hydroxycarbonate chemically analogous to azurite ($Cu_3(CO_3)_2(OH)_2$), while green verditer has long been understood to be chemically analogous to malachite, a copper hydroxycarbonate with alternative stoichiometry ($Cu_2CO_3(OH)_2$). This work, however, identifies for the first time a copper hydroxynitrate, rouaite ($Cu_2NO_3(OH)_3$), as the main product of laboratory-based replications of the historical verditer production process. Although this work does not directly address the identification of rouaite in historical samples, this is the subject of an additional forthcoming publication. One previous study (of an early seventeenth century miniature painting) has also identified rouaite as a pigment, although its origin is not investigated in detail [5].

Verditers are widely documented in written sources and historical works of art. Due to the expense of alternative blue pigments, the blue colour was much more valuable than the green [6, 7]. The earliest mention of 'verditer' occurs in 1506–1507. As the origin of the name likely derives from 'verd de terre', it is assumed that successful production of the blue pigment followed that of the green; the earliest possible mention of blue verditer, 'verditer bis',[1] occurs in 1537–1538 [8, 9].

Verditer or verditer-like pigments have been identified throughout England (and continental Europe) [10–15]. Visual identification in English wall paintings and easel paintings from the sixteenth and seventeenth centuries is common, consistent with the earliest references to blue verditer in surviving records in the 1530s [6, 8, 16, 17].

Blue verditer, identical to azurite when studied by PXRD and Raman spectroscopy, is distinguished from naturally produced azurite by its specific morphology and lack of diverse associate minerals common to natural pigments. Since it is synthesized by precipitation from solution, it exhibits a distinct round shape and consistent, small particle size [6, 8, 11, 18]. It appears highly birefringent and lobed under polarized light [6, 18]. By-products of synthesis such as unreacted calcium carbonate, a synthetic reagent, may be present [19–21]. Natural calcium carbonate is also a common associate mineral of natural azurite and its presence should not be used to definitively draw conclusions about pigment origin [20, 21].

Several common associate minerals of naturally occurring azurite such as earth pigments, cerussite, and kaolinite were also used as pigments or extenders; their presence should not be used to conclusively decide a natural origin. Occurrence of a blue copper carbonate pigment absent of any of these species, however, suggests that the pigment possesses a synthetic origin. Characterisation of impurities and by-products resulting from verditer synthesis may also be useful to conservators in identifying extenders and degraded pigments originally present [11, 22].

The interpretation of the original colour of areas painted with verditers is challenging for conservators. Synthesis produced a range of colours from green to blue. Additionally, verditers were often mixed with organic yellow pigments that are difficult to detect and prone to fading. Yellowing of the medium over time may also make a blue pigment appear greener [11, 22]. Further scientific work on synthetic procedures and degradation reactions is therefore of great value.

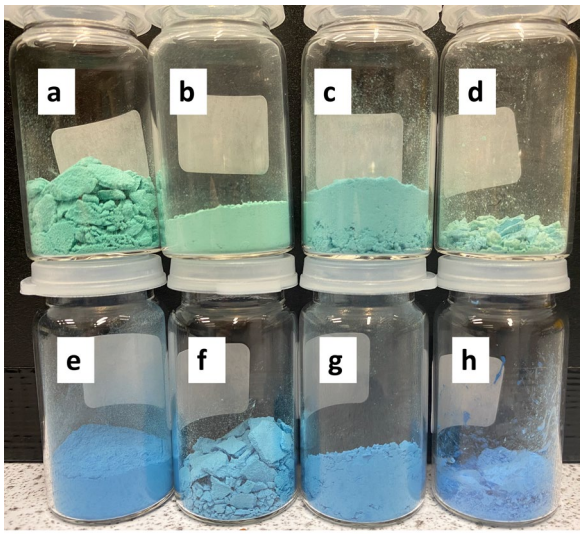

Fig. 1 Verditer synthesis under varying experimental conditions produces a range of colours due to varying proportion of two mineral species, verditer and rouaite ($Cu_2(NO_3)(OH)_3$); **a** Rx_Air_50_int. **b** Rx_Air_4_S1. **c** Rx_N2_20_cont. **d** Rx_Air_20_S3. **e** Rx_Air_4_int, three washes. **F** Rx_Air_20_int. **g** Rx_Air_20_int. **h** Rx_CO2_20_cont. Note that all products are named according to synthesis conditions as outlined in Table 2

Early discussions of verditer synthesis

Early modern synthesis of blue and green verditer was widely understood at the time to be unreliable, with small variations in synthetic procedure resulting in products spanning from green to blue, as shown in Fig. 1 [6, 10]. Nonetheless, this affordable pigment was evidently widely used, particularly in England [16, 23–25]; later treatises note that it was useful for producing vibrant greens when mixed with organic yellow pigments [11,

[1] 'Bis' and 'bys' were used earlier to describe a pigment as 'dark' and it is possible that this reference is to a deep or dark green pigment [68].

26]. Its ease of acquisition is reflected in the multiple accounts detailing the procedures for synthesis.

Verditer was produced from copper–water, a byproduct of the refining industries wherein nitric acid (aqua fortis) and copper metal reacted to form copper nitrate. Refiners' operations were often small scale and verditer production tended to be a secondary source of income [7]. Christopher Merrit's *The Art of Refining* (1677–78), describes the process:

> *'They put into a Tub a Hundred Pound weight of Whiting, and thereon pour the Copper- Water, and stir them together every Day, for some Hours ... when the Water grows pale, they take it out, and set [it] by for farther Use, and pour on more of the Green Water; and so continue till the Verditer be made...' [27]*

Other sources include John Harris (early 1700s) and Robert Dossie (1758), providing similar procedures [26, 28]. Robert Boyle (1669) tells of successful synthesis by heating the solution before reacting it with whiting [29]. Boyle may have been intentionally misled by a refiner looking to protect trade secrets [6]. The problem of unreliability was paramount for verditer producers, as Merrit notes in his appendix to a translation of an Italian glass-making treatise published in 1662: 'they can assign no reason, nor can they hit on a certain rule to make constantly their Verditer of a fair Blew, to their great disprofit, the Blew being of manifold greater value than the Green.' [30]

Further complicating the discussion of verditer synthesis is evidence of many other syntheses for blue pigments, likely cuprammonium salts, dating back as far as the eighth century [31–35]. These syntheses are outside the scope of this work and products have not been detected in many surviving samples, though the possibility of their use should not be ruled out.

Previous scientific research

MacTaggart & MacTaggart studied the products of historical verditer syntheses in 1980, which provided a basis for this work. The green and blue synthetic products were characterized by polarised light microscopy (PLM). They found that the product colour was dependent on the synthesis temperature; the blue product was not formed above 12°C, a result that this work brings into question [6].

This led to the hypothesis that the success of the English verditer industry was due to cold English winters, while syntheses were not successful during warmer months. Historians have cited this work to explain why the English verditer industry succeeded where those in warmer continental Europe failed [8]. The mechanism for successful blue verditer synthesis, however, has not yet been elucidated, and has important implications for the historical understanding of pigment production and availability in the early modern period.

Objectives and impact of research

Although previous scientific research has investigated the products of the 'refiners' verditers' synthesis method, the products of this synthetic procedure have not been previously characterised by chemically specific analytic methods. This work combines visual analysis, electron microscopy (SEM), Raman spectroscopy, and Powder X-Ray Diffraction (PXRD) to study the products of verditer synthesis.

The objectives of this work, therefore, is to address these open questions:

- What products are formed in the "refiners' verditers" synthesis?
- Does the identity of products explain variation in colour?
- Is it possible to identify plausible reaction mechanism(s), and explain the dependence on various experimental/environmental variables?
- Do the variables controlling product outcomes suggest any historical influences leading to successful or unsuccessful verditer production, and are these in turn supported by primary source material?

The products formed in these reactions are also relevant as copper corrosion products in both industrial and archaeological settings [36–41], and as synthetic catalyst precursors for mediation of various chemical contaminants [42–47]. Their formation and reactivity under a range of reaction conditions, subject to significant debate in the literature, is therefore relevant beyond the area of pigment studies [39, 48, 49].

The use of 'verditer' throughout the text refers to blue verditer, the synthetic analogue of azurite. Azurite refers to the naturally occurring mineral. 'Green verditer' indicates the green synthetic pigment often previously identified as synthetic malachite, instead found here to be rouaite, a synthetic copper nitrate. It is important to note that blue verditer and azurite (and similarly, synthetic malachite and malachite) share the same Raman spectra and powder X-Ray diffraction patterns, and therefore, reference data from the American Mineralogist Crystal Structure Database (AMSCD) for azurite and malachite are referenced throughout the text under the mineral names. The terminology has been chosen to reflect the historical texts and previous scientific work on these materials and to minimise confusion. Table 1 summarises the nomenclature used in this work.

Table 1 Summary of nomenclature

Name	Description
Azurite, malachite	Natural copper hydroxycarbonate minerals
Blue verditer	Synthetic copper hdroxycarbonate chemically analogous to azurite
Green verditer	Green synthetic pigment material produced as byproduct of blue verditer synthesis; identity uncertain
Synthetic malachite	Synthetic analogue of malachite
Synthetic azurite	Synthetic analogue of azurite produced outside of context of pigment synthesis (ie in literature studies of thermodynamic stability)

Table 2 Summary of synthetic routes studied

Name	T (℃)	Atmosphere	Stirring	Copper source	Carbonate source	Product(s)
Rx_Air_4_int	4	Air	Intermittent	0.31 M $Cu(NO_3)_2 \cdot 3H_2O$	0.31 M $CaCO_3$	Rouaite, verditer
Rx_Air_20_int	20	Air	Intermittent	0.31 M $Cu(NO_3)_2 \cdot 3H_2O$	0.31 M $CaCO_3$	Rouaite, verditer, trace malachite
Rx_Air_20_cont	20	Air	Continuous	0.31 M $Cu(NO_3)_2 \cdot 3H_2O$	0.31 M $CaCO_3$	Rouaite, verditer
Rx_Air_50_int	50	Air	Intermittent	0.31 M $Cu(NO_3)_2 \cdot 3H_2O$	0.31 M $CaCO_3$	Rouaite
Rx_N2_20_cont	20	100% N_2 at 1 atm	Continuous	0.31 M $Cu(NO_3)_2 \cdot 3H_2O$	0.31 M $CaCO_3$	Rouaite
Rx_CO2_20_cont	20	100% CO_2 at 1 atm	Continuous	0.31 M $Cu(NO_3)_2 \cdot 3H_2O$	0.31 M $CaCO_3$	Azurite
Rx_CO2Var_20_cont	20	Variable CO_2 concentration	Continuous	0.31 M $Cu(NO_3)_2 \cdot 3H_2O$	0.31 M $CaCO_3$	Rouaite
Rx_Air_20TC_cont	20	Air	Continuous	0.31 M $Cu(NO_3)_2 \cdot 3H_2O$	0.31 M $CaCO_3$	Rouaite, verditer
Rx_Air_20TC_int	20	Air	Intermittent	0.31 M $Cu(NO_3)_2 \cdot 3H_2O$	0.31 M $CaCO_3$	Rouaite, verditer, trace malachite
Rx_Air_50TC_cont	50	Air	Continuous	0.31 M $Cu(NO_3)_2 \cdot 3H_2O$	0.31 M $CaCO_3$	Rouaite
Rx_Air_50TC_int	50	Air	Intermittent	0.31 M $Cu(NO_3)_2 \cdot 3H_2O$	0.31 M $CaCO_3$	Rouaite, trace malachite
Rx_SynAir_20TC_cont	20	Synthetic air (80/20 N_2/O_2)	Continuous	0.31 M $Cu(NO_3)_2 \cdot 3H_2O$	0.31 M $CaCO_3$	Rouaite, trace verditer
Rx_SynAir_20TC_int	20	Synthetic air (80/20 N_2/O_2)	Intermittent	0.31 M $Cu(NO_3)_2 \cdot 3H_2O$	0.31 M $CaCO_3$	Rouaite
Rx_Air_4_S1	4	Air	Intermittent	0.078 M $Cu(NO_3)_2 \cdot 3H_2O$	0.31 M $CaCO_3$	$CaCO_3$ (first wash), malachite (second wash)
Rx_Air_4_S2	4	Air	None	0.31 M $Cu(NO_3)_2 \cdot 3H_2O$	0.31 M $CaCO_3$	Rouaite, azurite, malachite
Rx_Air_20_S3	20	Air	Continuous	0.31 M $Cu(NO_3)_2 \cdot 3H_2O$	0.31 M Na_2CO_3	Rouaite
Rx_Air_20_S4	20	Air	Continuous	0.31 M $Cu(NO_3)_2 \cdot 3H_2O$	0.31 M $CaCO_3$, ultrapure H_2O	Rouaite
Rx_Air_20_S5	20	Air	Continuous	0.31 M $CuSO_4 \cdot 5H_2O$	0.31 M $CaCO_3$	Devilline, $CaCO_3$, gypsum, posnjakite

Experimental

Synthesis reactions

All reaction procedures studied are summarised in Table 2, and products are named and referred to throughout the text according to the relevant reaction conditions used.

Reference materials

A reference sample of commercially produced blue verditer was purchased from L. Cornellisen & Son and compared to lab synthesized pigment samples. Reference samples of green verditer and natural malachite were obtained from Dr. Andrea Kirkham.

Standard synthesis following procedure of MacTaggart & MacTaggart: Rx_Air_4_int

0.31M Solid copper nitrate trihydrate (Scientific Laboratory Supplies, > 98% purity) was dissolved in deionised water in a wide-mouthed glass jar by stirring with a magnetic bar. While solution was stirred, 0.3M solid calcium carbonate (Acros Organics, 99% extra pure) was added (Table 1). The solution was stirred for seven hours either

at a constant rate or intermittently (for one minute every 20 min).

Following the first 7 h reaction, the solution was stirred twice in the next 24 h. The solid product was then filtered using a Buchner funnel and filter paper and rinsed with deionised water. Subsequent reactions, referred to in the text as second and third washes, of the same product were then carried out, in which additional new calcium carbonate and copper nitrate solution in the same concentrations and quantities as in the first reaction were added to the product and reacted under the above procedure. This process followed the historical procedure outlined by Merrit in *The Art of Refining*.[27]

The final product was then filtered using a Buchner funnel and filter paper, rinsed with deionised water, and dried prior to analysis.

Additional reaction routes are presented in detail in Additional file 1 and summarised in Table 2.

Thermal control

Reactions were carried out at several temperatures. Hot conditions were created by carrying out reaction on a heated stir plate (Rx_Air_50_int). Temperatures were monitored and observed to fluctuate between 45 and 55 °C. Cold conditions were created by placing the stir plate and vessel inside a refrigerator at 4 °C (Rx_Air_4_int). For reactions carried out at room temperature (Rx_Air_20_int, cont), we have reported the temperature as 20 °C throughout the text for the sake of consistency. The temperature of the laboratory underwent minor fluctuations between 17 and 21 °C.

Selected reactions at 20 °C and 50 °C were also replicated with thermal control to ± 0.1 °C using a thermometer with PID controller (IKA ETS D5). These are denoted by TC in name. Precise thermal control was not found to alter product identity or proportion.

Alteration of atmospheric composition

Rx_N2_20_cont. Removal of atmospheric CO_2 was carried out by two methods. A glove box containing reagents was purged with nitrogen. Then reagents were combined and allowed to react for seven hours followed by immediate filtration. The second method used an inlet line connected to dry nitrogen and an outlet line into a fume hood to purge the air in the reaction vessel (sealed using parafilm). Calcium carbonate was added quickly following purge and vessel was resealed. Reaction was then carried out followed by immediate filtration of products.

Rx_CO2_20_cont. Creation of a CO_2 atmosphere was carried out by installing an inlet line connected to a CO_2 cylinder and an outlet line into a fume hood in the space above the solution in the reaction vessel (Fig. 2). The chamber was sealed using parafilm and purged with CO_2 for 5 min, after which calcium carbonate was added, the vessel was resealed, and reaction was carried out under CO_2 flow (20 cm^3/min). The product at an intermediate time point, four hours, was sampled by removal of product suspended in solution from reaction chamber by needle followed by drying and analysis. After 7 h, the gas flow was stopped, the vessel unsealed, and the product filtered immediately.

Fig. 2 CO_2 atmosphere reaction vessel setup; inlet and outlet CO_2 lines are secured in vessel

Rx_CO2var_20_cont. For intermediate levels of CO_2 (9500, 20,000, and 50,000 ppm), multiples of a set volume of CO_2 (corresponding to 3500 ppm as measured using gas balloon and CO_2 monitor) was introduced into a sealed glove box and allowed to equilibrate (as evidenced by CO_2 monitor, RS Pro DT-802). The reaction was then carried out as described inside the glove box.

Rx_SynAir_20TC_cont, int. Selected reactions were also replicated under synthetic air. The ratio of N2:O2 was 80:20 (controlled using flow meters, 160 cm^3/min: 40 cm^3/min) with an overall flow rate of 200 cm^3/min and the same setup as that used for creation of CO_2 atmosphere.

Product characterisation

Characterisation by Raman spectroscopy

Raman spectra were collected using a Horiba LabRAM HR Evolution confocal Raman spectrometer, with a 50× microscope objective (Olympus LMPLFLN), a 600 grooves/mm grating, 100 µm pinhole, and a CCD array (Hamamatsu, 1024 × 1024 pixels). 532 nm excitation laser (diode-pumped solid-state, Laser Quantum) was selected based on superior S/N ratio with minimal sample damage per previous laboratory work and literature [50]. Spectra were collected at 10% or 25% ND filter (approximately 1.25 mW power at surface), 10s acquisitions, and 20 accumulations in the range 100–1800 cm^{-1}.

Spectra were processed using OriginPro 8 software. All spectra were fitted to a spline baseline, and anomalous noise peaks were removed in the spectra presented to aid in interpretation.

Characterisation by powder X-Ray diffraction

Powder X-Ray diffraction (PXRD) data were collected on a Malvern Panalytical Empyrean instrument, equipped with an X'celerator Scientific detector using non-monochromated CuKa radiation (l = 1.5418 Å). The sample was placed on a glass sample holder and measured in reflection geometry with sample spinning. The data were collected at room temperature over a 2q range of 3–80°, with an effective step size of 0.0167° and a total collection time of 60 min.

Characterisation of powder by scanning electron microscopy/energy dispersive X-Ray spectroscopy (SEM/EDX)

SEM images were collected on a TESCAN MIRA3 FEG-SEM at magnifications up to 40x. Samples were coated with platinum prior to imaging. Elemental mapping by EDX was carried out using a JEOL JSM-5510LV scanning electron microscope (backscatter electron detector, 20 mm working distance, 15 keV accelerating voltage) coupled to an Oxford instruments INCA EDX detector and software (version 4.01).

Colorimetry

Colorimetry data were collected using a Minolta CR-221 colorimeter with D65 illumination source in the CIELAB colour space. Three data collections were averaged for each sample and standard deviations are presented.

Results

Summary table of synthetic routes and resulting product(s)

The syntheses studied are summarised in Table 2, which details the reaction conditions as well as resulting products for each route. Reactions are named systematically and referenced throughout the text as such.

Initial results of syntheses: detection of an unexpected copper nitrate alongside blue verditer

Previous work reports the formation of a variety of products ranging in colour from green to blue [6]. This range was observed in repetitions of syntheses in this work as well, with most results under standard reaction conditions producing an intermediate blue-green product.

Characterisation of the product by Raman spectroscopy confirmed the presence of blue verditer ($Cu_3(CO_3)_2(OH)_2$) with characteristic bands at 400, 831, and 1090 cm^{-1}. Representative Raman spectra for samples synthesized under cold conditions with intermittent stirring are presented in Fig. 3. Unreacted calcium carbonate was also observed. In addition to blue verditer, a green basic copper nitrate was identified, rather than the expected malachite ($Cu_2CO_3(OH)_2$).

Careful analysis of Raman spectra as well as PXRD (Fig. 4) revealed that this compound was rouaite ($Cu_2NO_3(OH)_3$), the metastable monoclinic polymorph of gerhardtite that is most commonly observed in synthetic samples [51]. PXRD analysis additionally showed malachite present as a minor component, as well as unreacted calcium carbonate. Rouaite exhibits characteristic Raman bands at 404, 454, and 1046 cm^{-1} (marked ∗ in Fig. 3a), and can therefore be readily differentiated from verditer and synthetic malachite. Verditer, on the other hand, shows characteristic Raman bands at 400, 831, and 1090 cm^{-1} (marked + in Fig. 3a).

Microscopic analysis of samples, on the other hand, showed similarity between samples composed of primarily rouaite those composed of primarily verditer (Fig. 5). Examination of synthesized verditer/rouaite mixtures by polarised light microscopy, used in previous studies of these experiments to characterise blue and green verditer, showed structures in agreement with earlier studies of verditers as well as commercial verditer: small, lobed crystals that are highly birefracting [6].

Rouaite, with chemical formula $Cu_2(NO_3)(OH)_3$, has not been identified in reference synthetic green verditer samples studied previously (Additional file 1: Fig. S1), and has not been identified in historical wall painting samples to date, although in a later publication Mactaggart and Mactaggart suggested that the green synthetic product may be gerhardtite (rather than malachite) [53]. Rouaite has also been noted as a common impurity in the synthesis of other mixed-metal hydroxycarbonates, suggesting that its presence in this synthesis should not be unexpected [42].

Product morphologies were studied further by scanning electron microscopy of coated particles. Rouaite shows a distinct tabular morphology, and is readily differentiated from verditer, which appears as smaller intersecting plates forming roughly spherical aggregates (Fig. 6). The appearance of rouaite observed here is consistent with samples synthesised by precipitation published elsewhere [49]. The appearance of verditer is consistent with that of various reference samples that have been studied previously as part of ongoing work on its characterisation as well as results published elsewhere [6, 18, 19, 54, 55].

Products were more blue following subsequent reactions (second, third wash) of the same product in which additional unreacted carbonate and copper nitrate solution were added to product and reacted. Figure 7 shows the products resulting from one, two, and three washes with corresponding CIEL*a*b* colour values. After subsequent

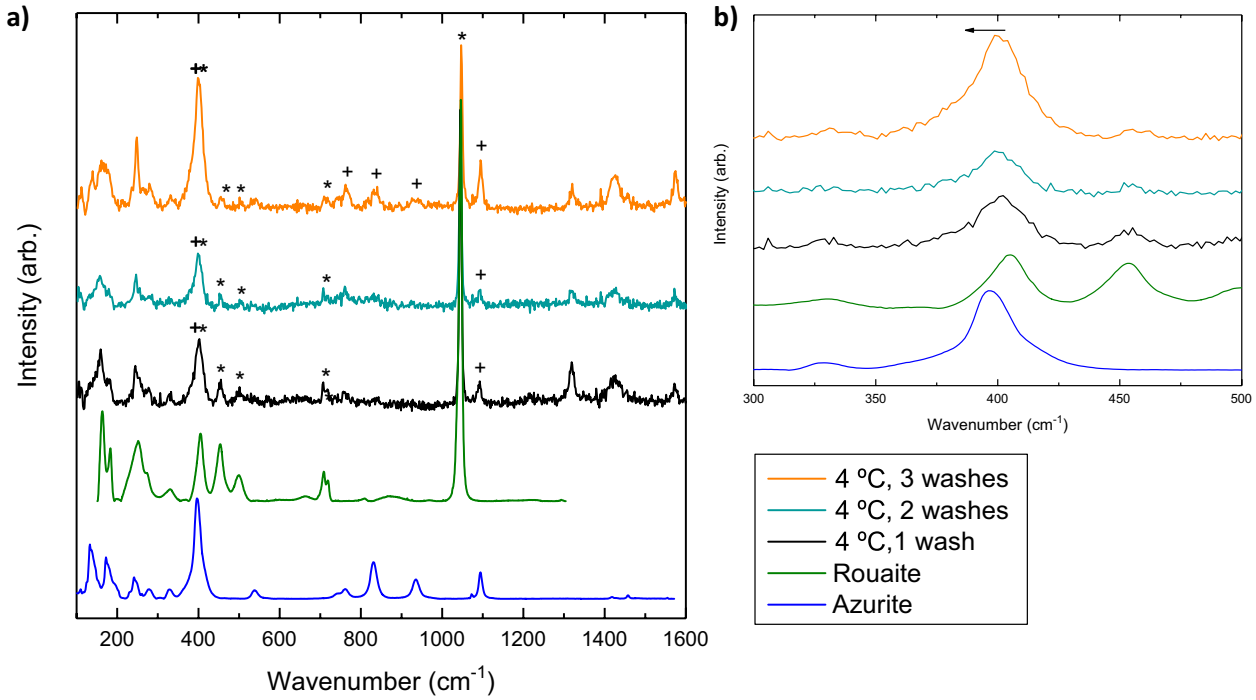

Fig. 3 **a** Representative Raman spectra of synthetic samples (Rx_Air_4_int), following one (black), two (teal), or three (orange) washes. Reference spectra for rouaite (green) and azurite/verditer (blue) are provided for comparison [52]. Significant bands of rouaite (*) and azurite/verditer (+) are marked. The convoluted band at 400/404 cm^{-1} as well as significant rouaite (454, 1046) and azurite/verditer bands (831, 1090) are labelled. **b** The shift of the convoluted 400/404 cm^{-1} band following subsequent washes is shown, indicating a more significant contribution from verditer after subsequent washes

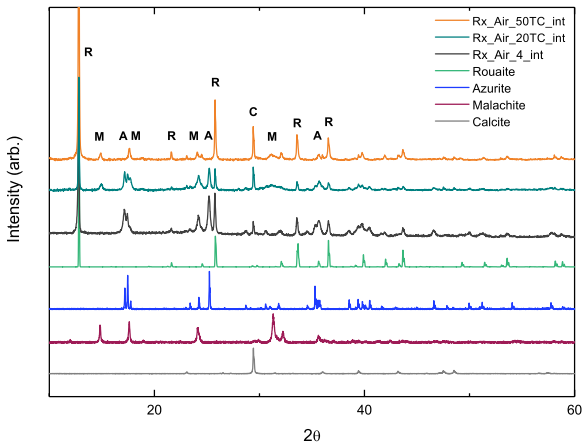

Fig. 4 PXRD diffraction patterns of synthetic samples Rx_Air_4_int (black); Rx_Air_20TC_int (teal) and Rx_Air_50TC_int (orange) conditions are shown. Reference patterns for rouaite (green), azurite/verditer (blue), malachite (red), and calcite (grey) are provided for comparison [52]. Significant bands of rouaite (R), azurite/verditer (A), malachite (M), and calcite (C) are marked

washes, there is a shift to more negative b* (more blue) and less negative a* (less green). While this multistep procedure was initially studied due to its presence in verditer recipes, these results led to a crucial hypothesis about the synthetic mechanism.

The result suggests that the formation of verditer proceeds via a gradual displacement following initial formation of rouaite. The shift in relative verditer proportion was confirmed by PXRD of products following one, two, and three subsequent reactions (Fig. 7). Integrated peak area ratios presented in the inset table in Fig. 8 confirm that, following subsequent washes, azurite increases in abundance relative to rouaite in the product. This is consistent with visual and colorimetric examination of products (Fig. 7 and Additional file 1: Table S2), allowing the use of colour as a proxy for relative phase composition.

The conversion of rouaite to verditer is dependent upon the replacement of nitrate anions with carbonate anions. It was therefore proposed that the synthesis may be influenced by the concentration of carbonate anions in solution and therefore the carbonate-carbon dioxide equilibrium as shown in the following reactions:

$$CO_3^{2-} + H^+ \rightarrow HCO_3^- \quad (1)$$

$$HCO_3^- + H^+ \rightarrow CO_2 + H_2O \quad (2)$$

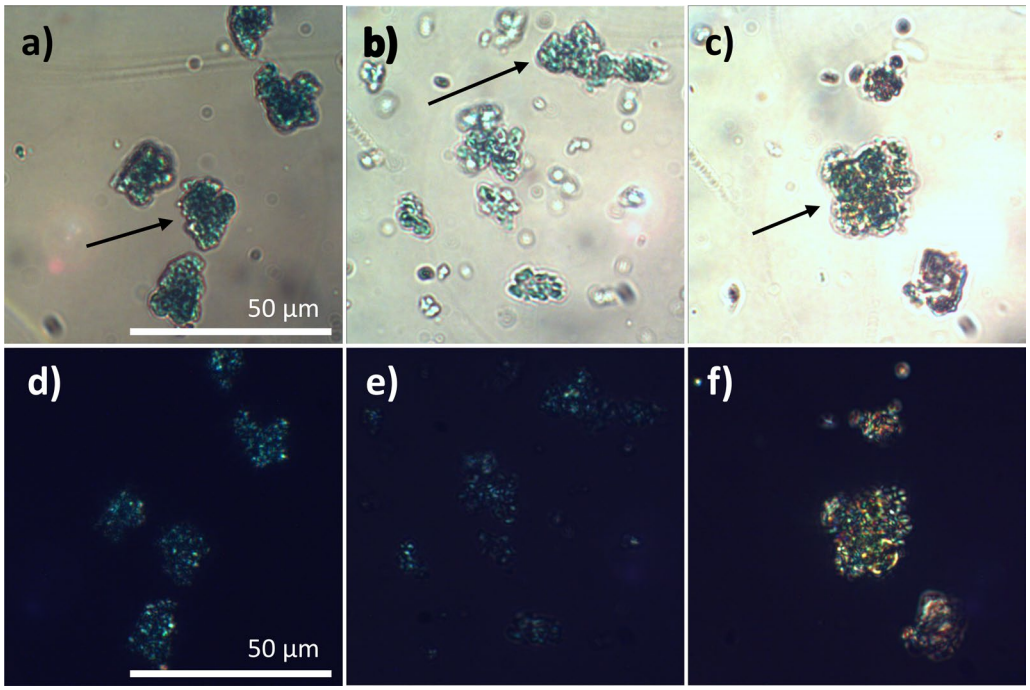

Fig. 5 PLM images in light field and through crossed polars of **a**, **d** Commercial blue verditer (L. Cornellisen); **b**, **e** Rx_Air_4_int, three washes, blue verditer; **c**, **f** Rx_Air_4_S2, synthetic rouaite/ blue verditer/malachite. Note lobed "cauliflower" structure and birefringence under crossed polars consistent with earlier literature on verditer and verditer-like pigments [6, 18]

This equilibrium is dependent on factors such as partial pressure of carbon dioxide (pCO_2) and solution pH.

The conversion of rouaite to verditer may be analogous to 'hydroxy double replacement reactions' in which anions in a layered salt structure are loosely bound and therefore readily exchanged. Rouaite has been used as a precursor to synthesise organometallic catalysts in which nitrate anions are replaced by organic anions [49, 56, 57].

While nitrate anions are loosely bound in layered hydroxy salts (Fig. 9a), the larger negative charge of carbonate anions means that they are not readily exchanged once bound within the crystal structure. Figure 9b shows the crystal structure and bonding in azurite/verditer, in which carbonate anions are multiply bound to nearby copper ions; it is apparent that this crystal structure is radically different, a possible explanation for the irreversibility observed.

Several other copper minerals (including langite, botallackite, and paratacamite) as well as organometallic catalysts form via facile ion exchange with rouaite, in which loosely bound intercalated nitrate anions are exchanged for loosely bound chloride and sulphate anions [49]. The original crystal habit, or shape, is often maintained in the product [48, 49, 58].

It is also possible that conversion occurs via dissolution and recrystallization [49]. The structural similarity of azurite to rouaite, both in terms of lattice parameters and bonding of carbonate anion, is low, as observed in Fig. 9, suggesting that dissolution and recrystallisation is more likely than anion exchange [49, 59]. In this case, the structural and electronic differences between rouaite and azurite still hold as an explanation for the irreversibility for conversion.

Effect of temperature: results inconsistent

Initial work focused on the possible thermal dependence proposed by MacTaggart & MacTaggart and widely accepted as an explanation for the superior quality of English blue verditer over French verditer produced in the early modern period [6, 8, 9, 24]. Reactions at ambient room temperature (approximately 20 °C) produced mixtures of rouaite and verditer in varying proportions (Fig. 10, Additional file 1: Table S2). Intermittent stirring slightly favoured verditer formation compared to continuous stirring, but this is inconsistent as well.

Although the variability of results suggests that temperature may play a minor role in the successful production of blue verditer, it did not control the synthetic outcome and does not explain why the reaction succeeds or fails. A cooler climate (therefore colder reaction temperatures) does not explain the production of a blue product rather than a green one.

The effect of raising the temperature to 45–55 °C was then evaluated. This produced primarily rouaite with

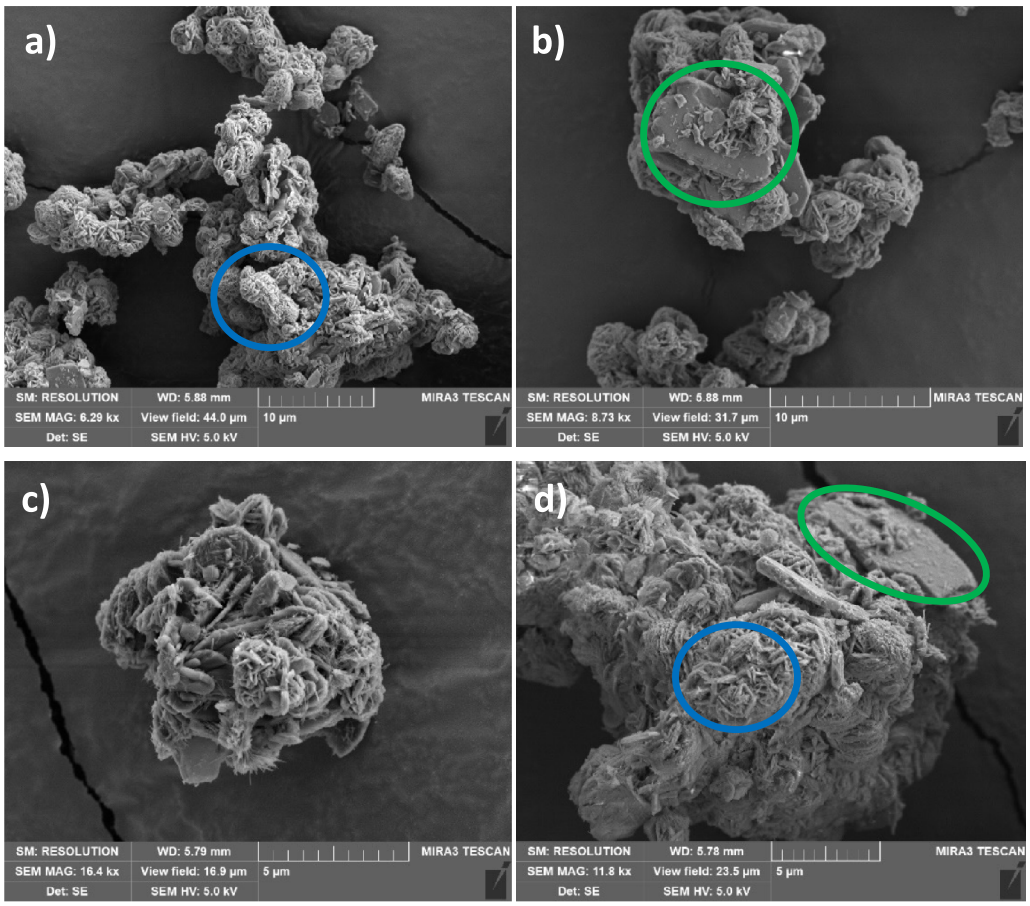

Fig. 6 **a**, **b**: Rx_Air_4_int; **c**, **d** Rx_Air_20_int. Verditer morphology circled in blue. Rouaite morphology circled in green

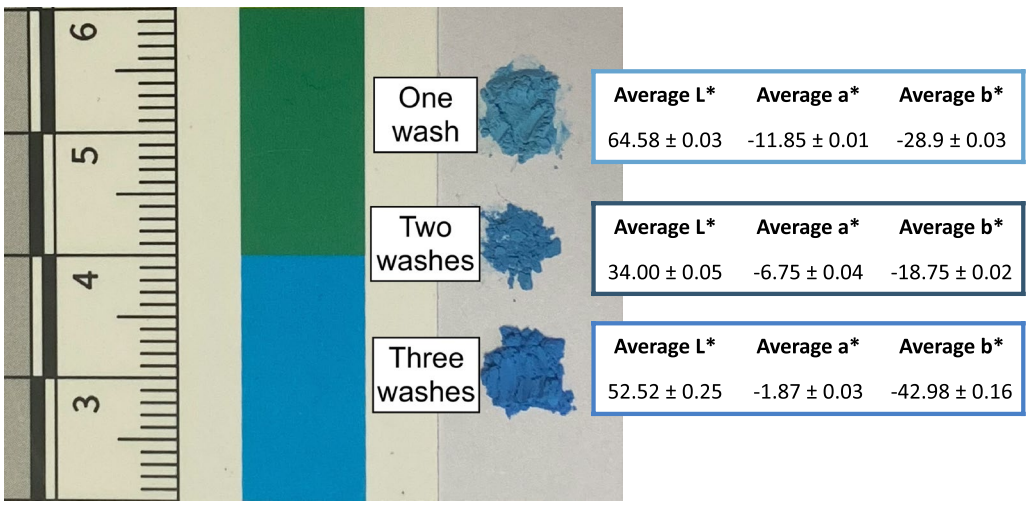

Fig. 7 Photograph of Rx_Air_4_int following one, two, and three washes with CIELAB coordinates for products from one and three washes. Average L*, a*, and b* values and standard deviations from three data collections are presented for each product

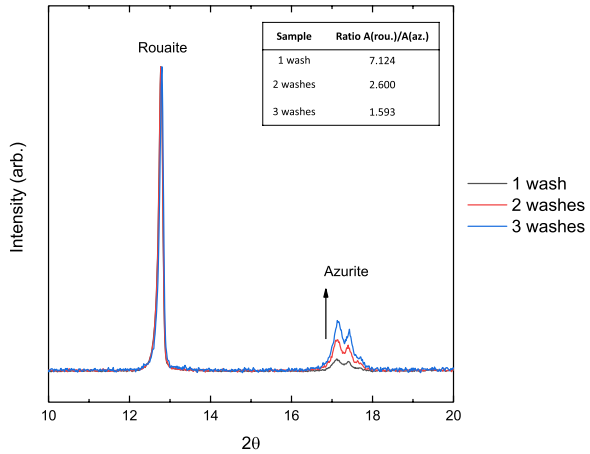

Fig. 8 PXRD patterns of Rx_Air_4_int after first, second, and third washes. Data are normalized to the intensity of the rouaite peak at 12.8, and peak intensities of verditer bands at 17.2 and 17.4 are observed to increase following the second and third washes. Inset table provides the integrated peak area ratio A(rouaite)/A(azurite) determined by integrating the peak areas (12.0–13.25 2θ for rouaite, 16.5–18.0 2θ for azurite) from the non-normalised patterns for each sample. The integrated peak area ratios similarly show increasing azurite content relative to rouaite following subsequent washes

traces of malachite, suggesting that there is a temperature threshold above which verditer production is disfavoured, although this is well above the range of historical ambient air temperatures in England (not exceeding an average of 20 °C in summer and not falling below an average of 3 °C in winter during the sixteenth and seventeenth centuries) [61, 62].

The effects of temperature are still not fully explained. There was significant variability in the hue and relative proportion of verditer/rouaite of products produced at the same temperature and reaction conditions (Fig. 10). It was therefore proposed that temperature may play a role in influencing another factor not previously identified. As solution equilibria may be perturbed by temperature changes, and the rouaite to verditer conversion reaction is dependent on ion concentrations, the influence of carbon dioxide partial pressure (pCO_2) and therefore carbonate ion concentration was investigated.

Effect of atmospheric carbon dioxide concentration: is control over bicarbonate equilibrium the key?

Variation in the atmospheric pCO_2, an equilibrium sensitive to environmental factors such as temperature, was therefore proposed to influence the carbonate ion availability in solution and therefore verditer production. Initially, extreme conditions were used to study the reaction under very low (nitrogen atmosphere) and very high pCO_2 values (100% CO_2 at 1 atm).

Some verditer formed in very low abundance alongside mainly rouaite under a nitrogen atmosphere (approximately zero pCO_2) and under a synthetic air atmosphere (80% N_2, 20% O_2). The absence of CO_2 in the atmosphere disfavours the presence of carbonate in solution and favours production of carbon dioxide. Raman and PXRD data confirm the presence of primarily rouaite, as presented in Fig. 11. This result, though not historically relevant, is extremely useful in understanding the mechanism of synthesis. It suggests that successful verditer synthesis requires high carbonate concentration in solution, beyond that generated by dissolution of calcium carbonate, while rouaite formation occurs regardless. We note that reaction under synthetic air produces very slightly more verditer (Fig. 11b), which may suggest that stability and reactivity of rouaite are dependent on oxygen levels as well, although further work is necessary to comment on this conclusively.

Extremely pure verditer was observed after reaction under 100% CO_2 at 1 atm. This product was identified by Raman and PXRD analysis (Fig. 12). Rouaite is present after 4 h reaction time (sampled by removal of product suspended in solution from reaction chamber by needle) and absent by 7 h; this suggests that the mechanism of formation of verditer is not altered, but rather, the conversion of rouaite to verditer is greatly facilitated by increased pCO_2. Visually, the product is a deep blue colour (Fig. 2).

At lower, but still elevated relative to atmospheric, concentrations of CO_2 (9500, 20,000, 50,000 ppm), however, rouaite was still the major product of the synthesis based on PXRD analysis at room temperature after 7 h as shown in Fig. 13. It is therefore likely that elevated atmospheric CO_2 alongside additional factors influencing carbonate concentration would be necessary to definitively control synthesis.

Discussion

The concentration of carbon dioxide in the air above the open reaction vessel was found to significantly affect the composition of products. Verditer formation was facilitated by running reaction under 100% CO_2 at 1 atm, and suppressed by purging with N_2, removing atmospheric CO_2 as well as any evolved during the reaction. Although verditer formation was suppressed above 45°C, typical ambient temperature fluctuations corresponding to climatic variation in seventeenth century England (4°C for cold synthesis up to 17–20 °C, laboratory room temperature) did not influence the results. When verditer formation was suppressed, rouaite formed as an insoluble metastable product and was isolable. The conversion of verditer to rouaite was not observed, suggesting that

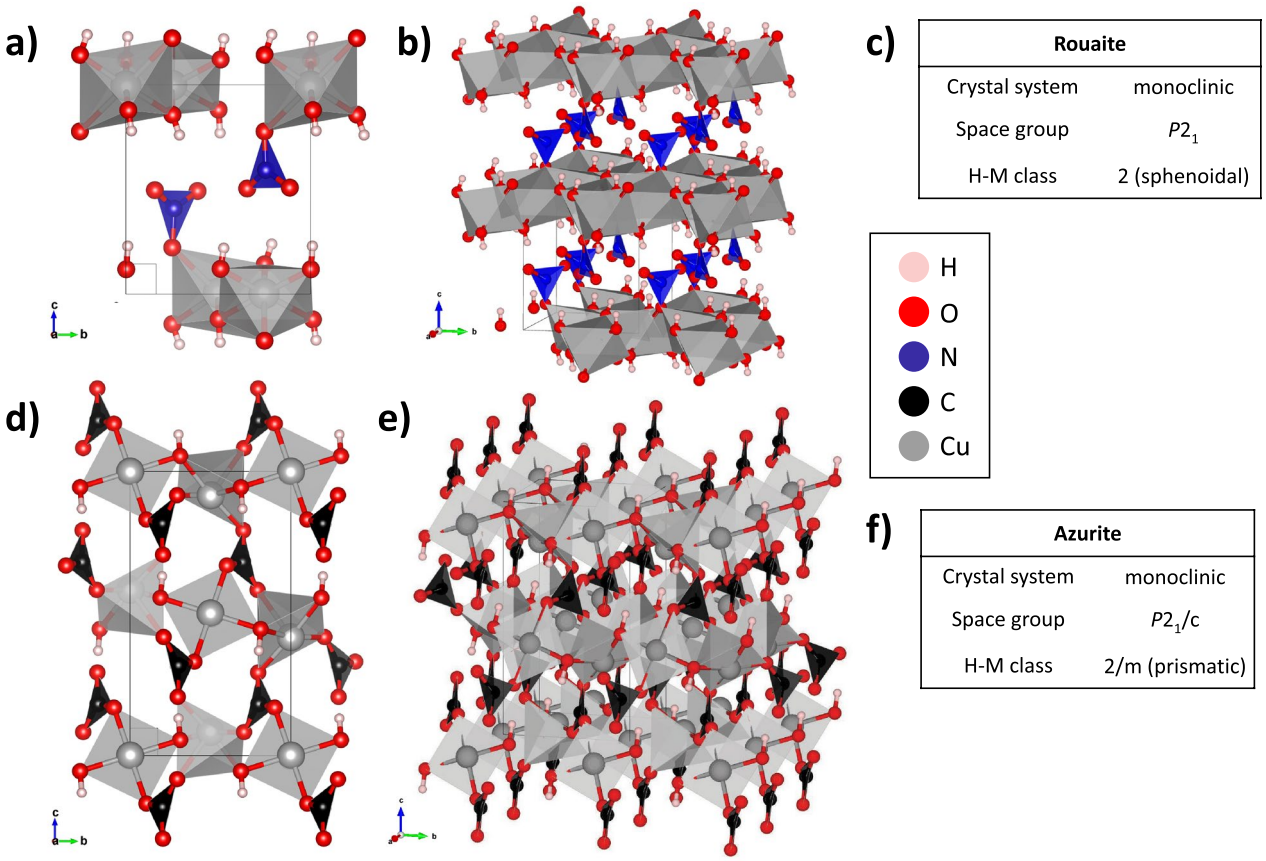

Fig. 9 Crystal structures and information for **a**–**c** rouaite and **d**–**f** azurite. Nitrate ions in rouaite are singly bound to copper ions and located in intercalated layer. Carbonate anions in azurite are multiply bound to copper above and below. Structures visualised using VESTA (Version 3.5.8) [60] and data from the American Mineral Society Crystal Database [59]

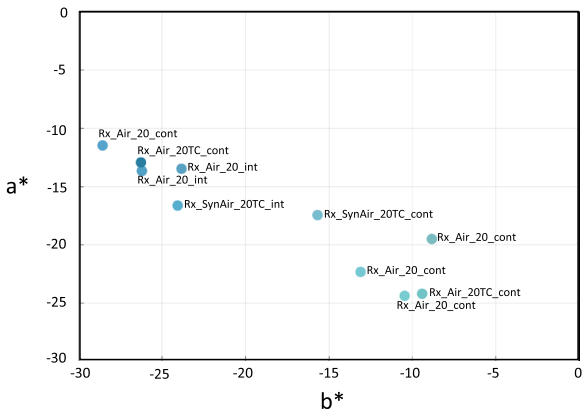

Fig. 10 Average CIELAB values a* (red-green) and b* (blue-yellow) for ten samples synthesised at 20 °C (continuous stirring, 0.31M $[Cu^{2+}]$, in air). Each sample data point is plotted in the corresponding colour value to aid in interpretation. Full colorimetry results are presented in Additional file 1: Table S2

verditer is significantly more stable than rouaite and the reverse reaction is unlikely to occur.

Perturbations to the bicarbonate-carbon dioxide equilibrium significantly affect the composition of products, and may explain the unreliability of historical verditer synthesis [6, 29, 30]. There are several competing reactions occurring in solution, with reversible reactions indicated by double headed arrows:

Formation of rouaite:

$$2Cu^{2+} + 3OH^- + NO_3{}^- \rightarrow Cu_2(NO_3)(OH)_3 \quad (3)$$

Rouaite to azurite:

$$3Cu_2(NO_3)(OH)_3 + 4CO_3^{2-} \rightarrow 2Cu_3(CO_3)_2(OH)_2 + 3NO_3^- + 5OH^- \quad (4)$$

Rouaite to malachite:

$$Cu_2(NO_3)(OH)_3 + CO_3^{2-} \rightarrow Cu_2(CO_3)(OH)_2 + NO_3^- + OH^- \quad (5)$$

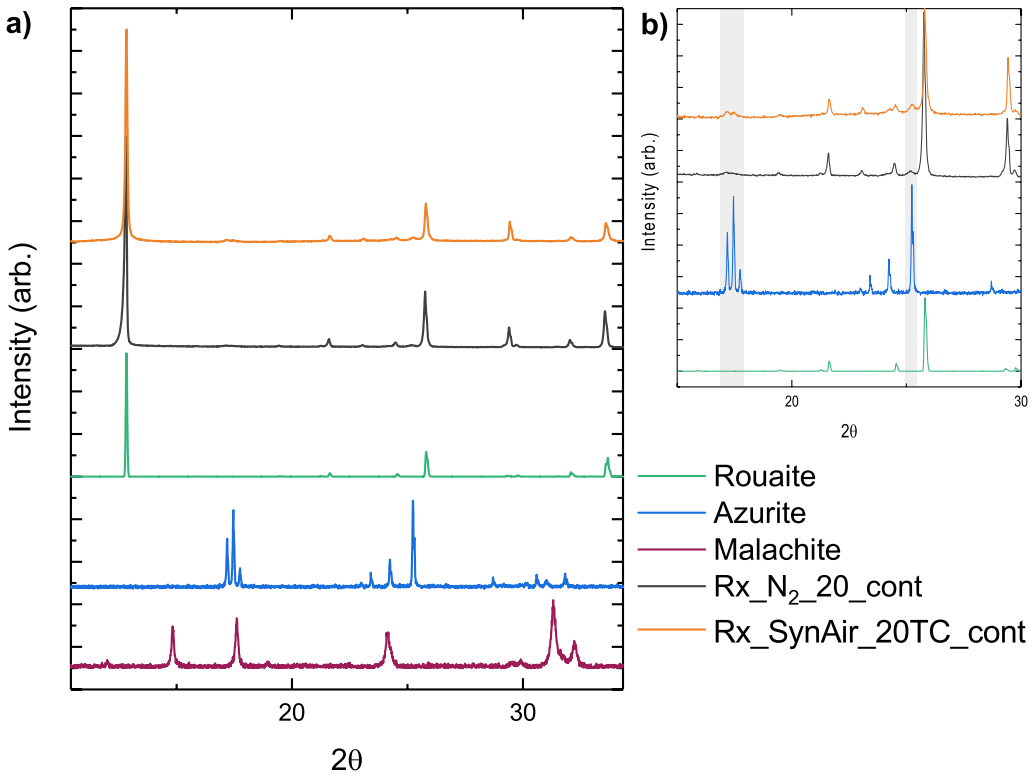

Fig. 11 **a** PXRD results of Rx_N2_20_cont (black) and Rx_SynAir_20TC_cont (orange) with verditer, rouaite, and malachite patterns provided for comparison [52]. The two conditions produce very similar patterns which correspond closely with reference for rouaite. **b** A smaller region of the PXRD pattern is shown, with grey regions highlighting very weak peaks in samples 1–3 corresponding to verditer [52]

Azurite to malachite:

$$2Cu_3(CO_3)_2(OH)_2 + 2H_2O \rightarrow 3Cu_2(CO_3)(OH)_2 + HCO_3^- + H^+ \quad (6)$$

Bicarbonate equilibrium:

$$CO_3^{2-} + 2H^+ \rightleftharpoons HCO_3^- + H^+ \rightleftharpoons CO_2(g) + H_2O \quad (7)$$

Dissolution:

$$CaCO_3(s) \rightleftharpoons Ca^{2+} + CO_3^{2-} \quad (8a)$$

$$H_2CO_3 \rightleftharpoons CO_2 + H_2O \quad (8b)$$

$$CaCO_3(s) + H_2CO_3 \rightarrow Ca^{2+} + 2HCO_3^- \quad (8c)$$

Carbon dioxide generation, favourable at low pCO_2 (here, when system is run under N_2), competes with the formation of blue verditer and synthetic malachite from rouaite in solution. At high pCO_2, the concentration of carbonate ions in solution increases; subsequently, rouaite is converted to verditer. Carbonate concentration is also dependent on the solubility of $CaCO_3$, which is low in water and decreases as temperature increases (e.g. from 5.26×10^{-4} M at 25 °C to 3.34×10^{-4} M at 55 °C in Coto et al. 2012) [63]. Higher pCO_2 (here, running the reaction at 20,000 ppm, 50,000 ppm, or 1atm CO_2), on the other hand, increases $CaCO_3$ solubility [63]. It should be noted that the temperature dependence of $CaCO_3$ solubility is strongly influenced by the temperature dependence of CO_2 solubility, which decreases at lower temperatures [63, 64]. High pCO_2 values are reported in previous analysis of natural azurite formation [58] and thermodynamic calculations [65], so this result is not unexpected. However, the CO_2 pressure required to attain complete conversion of rouaite to azurite in this work is much lower than those reported for formation of azurite from $Cu(NO_3)_2{\cdot}3H_2O$ [65].

There is some evidence from previous studies of patina formation that rouaite is formed readily at high temperatures (> 100 °C) [37, 38, 40]. Although the conditions of patina formation on a surface are significantly different to those of inorganic synthesis studied here, rouaite's stability as temperature is increased may help to explain the formation of pure rouaite at > 45 °C.

It is significant that verditer formation was not observed with a highly soluble carbonate, Na_2CO_3, which is also a stronger base. It is relevant to note that others

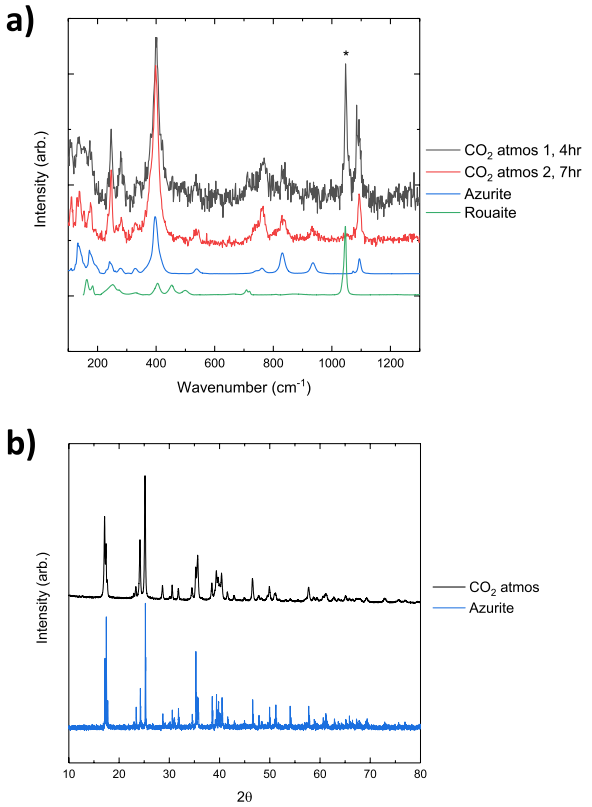

Fig. 12 **a** Raman spectra of Rx_CO2_20_cont sampled at 4 h (black) and 7 h (red). Reference Raman spectra of verditer (blue) and rouaite (green) are provided, and the strongest rouaite band at 1046 cm^{-1} is marked in the 4 h spectrum (*) [52]. **b** The PXRD pattern of the 7 h product is compared to the reference PXRD pattern for azurite/verditer, confirming the identity of the product as verditer with no detection of rouaite

have synthesized azurite ($CaCO_3$, RT, $pCO_2 = 5.0$ MPa for 48 h) and malachite (Na_2CO_3, 353K, pure CO_2 atmosphere) analogues from carbonates and copper nitrate, but at significantly higher pCO_2 values [65].

Malachite was not readily produced at the copper concentrations studied. Whilst malachite is more thermodynamically stable at low pressures of CO_2, these calculations assume equilibrium conditions [39, 48, 66]. This is a disequilibrium system, so we are wary of relying on these calculations to explain the products observed. We observed that synthetic malachite forms at lower Cu^{2+} concentrations, and in combination with rouaite and blue verditer when solutions were left undisturbed, suggesting that there may be some diffusion/mixing condition affecting its formation (see Additional file 1). It is not observed in most samples regardless of colour.

The mechanism of conversion from rouaite to verditer is also of significant interest, both in explaining the results and for work developing copper nitrate and carbonate catalysts. Conversion may occur via anion replacement or dissolution and recrystallisation. The crystal morphology observed does not clearly support one route over the other. Well-formed tabular rouaite crystals are present and do not appear to be disintegrating (Fig. 6), while verditer crystals form as rosettes or intersecting discs rather than tabular crystals. The relative abundance of rouaite decreases following subsequent reactions, however, suggesting that conversion is occurring. The dissimilarity in structure of the crystals and in the samples observed by SEM suggests that the likeliest explanation is dissolution–recrystallization, but further work would be useful to confirm this.

Conclusions

The results of this work represent a significant development in our understanding of English verditer synthesis as practiced during the early modern period, as well as of the synthesis and stability of basic copper nitrates and carbonates more generally. Synthetic conditions were examined to understand the influence of conditions that may have been relevant to the success or failure of verditer production historically as well as to clarify the sequence of reactions and byproducts formed. Although modern laboratory conditions cannot perfectly replicate those of pre-industrial production (and documentation of historical conditions is incomplete), it is nonetheless valuable to study verditer production using a combination of modern methods and attention to historical documentation [67].

The production of rouaite, an unusual basic copper nitrate previously unidentified as a verditer synthesis product, suggests that, in early modern English verditer production, green byproducts may have been composed of primarily rouaite and only occasionally malachite depending on synthetic conditions. Rouaite therefore may be a marker in historical samples for pigment produced by the refiners' synthesis. Rouaite has not been widely identified in historical samples to date, although it is relevant to note that it was detected in a miniature painting dated to 1617, used in combination with massicot to paint a green doublet [5]. Its presence in wall painting samples approximately dated to the period in which the refiners' synthesis is the subject of a forthcoming publication, in preparation.

The difficulty of detecting light elements using elemental analysis and its visual similarity to other green pigments in cross section may explain its sparse identification thus far. It is also possible that rouaite is highly susceptible to degradation over time; future work should address this issue. The identification of rouaite also challenges the widespread assumption that green verditer

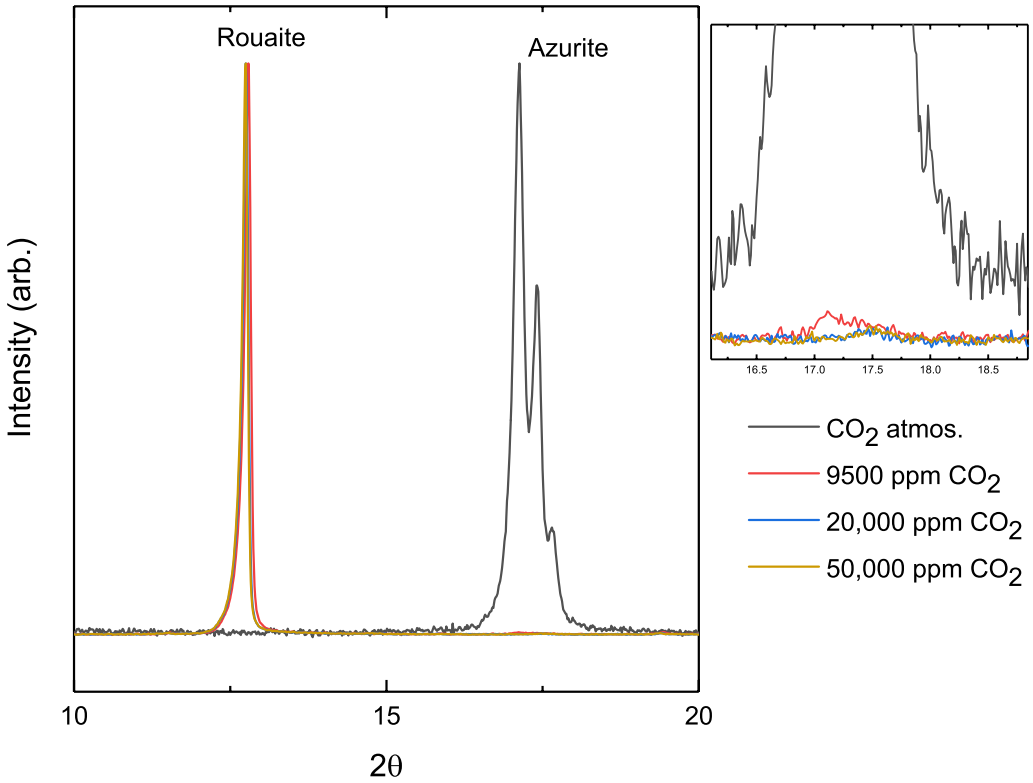

Fig. 13 PXRD patterns of Rx_CO2var_20_cont (black, 100% CO_2 at 1 atm; red, 9500 ppm; blue, 20,000 ppm; yellow, 50,000 ppm) at 20 °C, with continuous stirring. The dominant product for all lower pCO_2 values is rouaite. Inset shows zoomed in region of verditer peaks, emphasizing minimal verditer production at all values studied

pigment is comprised of the more stable basic copper carbonate, analogous to malachite.

The dependence of verditer colour on reaction temperature was found to be much weaker in this study than previously reported. Blue products were synthesized at ambient temperatures within the range of historical climatic variation in England. The success of English producers compared to those in continental Europe cannot be explained solely by direct climatic differences. Alternative explanations for the unreliability of the synthesis were therefore considered.

The synthesis was studied under a range of atmospheric gas concentrations, temperatures, concentrations, carbonate sources, and water sources. Factors influencing the concentration and availability of carbonate ions in solution were found to control the conversion of rouaite to blue verditer.

Most significantly, variation in the partial pressure of carbon dioxide during the reaction was found to affect the identity of the resulting product. At low concentrations of CO_2, blue verditer formation is suppressed, and the resulting product is primarily rouaite. At high concentrations of CO_2, the sole product is blue verditer. This effect is rationalised by an examination of studies on the stability of copper nitrate and carbonate and the complex chemical equilibria at play during this synthesis.

Although it is highly speculative, potentially significant variation in pCO_2 due to the location of synthesis and factors such as ventilation, indoor fires, and exhalation may have contributed to the observed unreliability of verditer synthesis. Documentation of refining procedures and workspaces in London and Sheffield, where verditer production is recorded, indicate that refining was done indoors in spaces often also containing smelting furnaces; this would have increased pCO_2 during synthesis, and these conditions may have been seasonally and regionally dependent [7, 69, 70]. Other historical factors influencing the carbonate equilibrium, such as local variations in water mineral content, may be of interest for further research.

This work represents a significant step in the understanding of verditer synthesis, and a novel contribution to literature regarding pigment synthesis and reproduction of historical recipes. Rouaite is reported for the first time as a major byproduct of blue verditer synthesis replications in the laboratory. Access to modern chemical analysis allowing the conclusive detection of rouaite

was critical to this work, showing the value of species and phase specific methods for researchers in heritage science.

Abbreviations

PLM	Polarised light microscopy
PXRD	Powder X-ray diffraction
SEM	Scanning electron microscopy
EDX	Energy dispersive X-ray spectroscopy
pCO_2	Partial pressure of carbon dioxide

Supplementary Information

The online version contains supplementary material available at https://doi.org/10.1186/s40494-024-01257-7.

Additional file1: Figure S1. Raman spectra (532 nm excitation) are presented for modern synthetic green verditer (red) and natural malachite pigment (blue). A reference spectrum for malachite is presented for comparison (black).[1] **Table S1.** Integrated areas and ratios of integrated areas A(rou.)/A(az.) from PXRD data collected from Rx_Air_4_int after one wash, two washes, and three washes. **Table S2.** Colorimetry values collected from reaction products. **Figure S2.** Two representative Raman spectra for samples synthesized at low [Cu2+] (black, red) are shown, with reference malachite (green) and calcite (grey) spectra provided for comparison. Significant peaks corresponding to malachite are marked by a circle (•), while significant calcite peaks are marked by a diamond (•). **Figure S3.** The PXRD pattern for one sample synthesized at low [Cu2+] is shown (black), with reference malachite (green) and calcite (grey) data provided for comparison. Significant peaks corresponding to malachite are marked by a circle (•), while significant calcite peaks are marked by a diamond (•). This confirms the presence of calcite and malachite and the absence of detectable azurite in low concentration samples. **Figure S4.** a) SEM image of low concentration product, boxed area is shown at higher magnification in b); c) EDX map of low concentration sample, showing Cu (red) and Ca (green) intensities. Particles of high Ca intensity suggest incomplete reaction of CaCO3. SEM images similarly show varied morphologies, including a fine, feathery structure in b). **Figure S5.** Representative Raman spectra for Rx_Air_20_S2 are presented, compared to literature spectra. Significant bands of rouaite (*), azurite (+), and malachite (•) are marked. Rouaite forms after the first wash (Unstirred 1, black). After the second wash rouaite (Unstirred 2, red), azurite (Unstirred 3, orange) and malachite (Unstirred 4, gold) are formed. Note that the gold spectrum for Unstirred 4 is a superposition of the azurite and malachite spectra, evident in the peaks around 400-430 cm^{-1}. **Figure S6.** Rx_Air_20_S2, allowed to react for several days without any disruption or mixing, <12 C. Distinct layers of green and blue are apparent, enclosed by white box. **Figure S7.** PXRD spectra of product resulting from reaction of Rx_Air_20_S5, CuSO4 starting material (1); reference spectra for devilline (2), posnjakite (3), gypsum (4), calcite (5). **Figure S8.** a) pH measurements over time recorded for DI H2O (black, red) and continuously stirred CaCO3 (blue, green) at room temperature and when heated. Note that room temperature sample experienced small increase in temperature generated from magnetic stirring action. b) pH measurements over time recorded for three samples of continuously stirred CaCO3 in Cu(NO3)2 solution, at room temperature (red), heated (black), and with increased total sample volume (blue). Elevated temperature does not significantly perturb pH for these samples.

Acknowledgements

We would like to acknowledge the financial support of the Gates Cambridge Trust, the ongoing support of Dr. Spike Bucklow, and the advice and feedback of Dr. Trevor Emmett and Camille Polkownik. We would also like to acknowledge the assistance of Dr. Chris Truscott in collecting PXRD data.

Author contributions

Theoretical conception: EP, AK, MC, SC; archival work: EP, SC; development of synthetic and analytic procedures and interpretation of results: EP, SC, MC; data presentation: EP, SC; writing: EP, SC; editing: EP, MC. All authors contributed to the final revision and reading of the manuscript.

Funding

This work was supported, in whole or in part, by the Bill & Melinda Gates Foundation [OPP1144]. Under the grant conditions of the Foundation, a Creative Commons Attribution 4.0 Generic License has already been assigned to the Author Accepted Manuscript version that might arise from this submission.

Availability of data and materials

The datasets used and/or analysed during the current study are available from the corresponding author on reasonable request.

Declarations

Competing interests

The authors declare no competing interests.

Received: 8 December 2023 Accepted: 22 April 2024
Published online: 02 May 2024

References

1. Cennini C. The craftsman's handbook: The Italian "Il Libro Dell'arte." Dover Edit. New York: Dover Publications; 1960.
2. Kirby J. The price of quality: factors influencing the cost of pigments during the Renaissance. In: Neher G, Shepherd R, editors. Revaluing Renaissance art. 2000. p. 19–42. (Routledge Revivals).
3. Nash S. Pour couleurs et autres choses prise de lui…": the supply, acquisition, cost, and employment of painters' materials at the Burgundian Court, c.1375–1419. In: Nash S, Kirby J, Cannon J, editors. Trade in artists' materials: markets and commerce in Europe to 1700. London: Archetype Publications; 2010. p. 97–182.
4. Kirby J. Trade in painters' materials in sixteenth-century London. In: Nash S, Kirby J, Cannon J, editors. Trade in artists' materials: markets and commerce in Europe to 1700. London: Archetype Publications; 2010. p. 339–55.
5. Burgio L, Cesaratto A, Derbyshire A. Comparison of English portrait miniatures using Raman microscopy and other techniques. J Raman Spectrosc. 2012;43(11):1713–21.
6. MacTaggart P, MacTaggart A. Refiners' verditers. Stud Conserv. 1980;25(1):37–45.
7. Wilson RE. Two hundred precious metal years; a history of the Sheffield Smelting Company Limited, 1760–1960. London: E. Benn; 1960.
8. Delamare F. Blue pigments: 5000 years of art and industry. London: Archetype Publications; 2013.
9. Harley RD. Artists' pigments c.1600–1835: a study in English documentary sources. 2nd ed. Artists' pigments c.1600–1835 : a study in English documentary sources. London: Butterworth Scientific; 1982. (Technical studies in the arts, archaeology and architecture).
10. Véliz Z. In quest of a useful blue in early modern Spain. In: Nash S, Kirby J, Cannon J, editors. Trade in artists' materials : markets and commerce in Europe to 1700. London: Archetype Publications; 2010. p. 389–400.
11. van Loon A, Speleers L. The use of blue and green verditer in green colours in the mid-seventeenth-century paintings of the Oranjezaal, The Hague. In: Spring M, editor. Studying old master paintings: technology and practice. Archetype Publications; 2011. p. 260–8.
12. Keith L. Giulio Romano and The Birth of Jupiter. Natl Gallery Tech Bull. 2003;24:38–49.
13. Vanmeert F, De Keyser N, Van Loon A, Klaassen L, Noble P, Janssens K. Transmission and reflection mode macroscopic X-ray powder diffraction imaging for the noninvasive visualization of paint degradation in still life paintings by Jan Davidsz. de Heem. Anal Chem. 2019;91(11):7153–61.
14. De Keyser N, van der Snickt G, Van Loon A, Legrand S, Wallert A, Janssens K. Jan Davidsz. deHeem (1606–1684): a technical examination of fruit and flower still lifes combining MA-XRF scanning, cross-section analysis and technical historical sources. Herit Sci. 2017;5(1):38.

15. Sperber R, Stenger J. Canaletto's Colour: the inspiration and implications of changing grounds, pigments and paint application in the artist's English period. Br Art Stud. 2016;https://doi.org/10.17658/issn.2058-5462/issue-02/rsperber-jstenger
16. Kirkham A. Sixteenth- and Seventeenth-Century Secular Wall Paintings in Suffolk, Vol. 1. The University of East Anglia; 2010.
17. Sheldon L. Palette, practice and purpose: pigments and their employment by native and Anglo-Netherlandish artists in Tudor and Jacobean painting. In: Cooper T, Burnstock A, editors. Painting in Britain 1500–1630: production, influences and patronage. Oxford: Oxford University Press; 2015. p. 128–37.
18. Roy A. Artists' pigments, vol. Two. Washington, DC: National Gallery of Art; 1993.
19. Švarcová S, Hradil D, Hradilová J, Čermáková Z. Pigments—copper-based greens and blues. Archaeol Anthropol Sci. 2021;13(11):190.
20. Aru M, Burgio L, Rumsey MS. Mineral impurities in azurite pigments: artistic or natural selection? J Raman Spectrosc. 2014;45(11–12):1013–8.
21. Smieska LM, Mullett R, Ferri L, Woll AR. Trace elements in natural azurite pigments found in illuminated manuscript leaves investigated by synchrotron X-ray fluorescence and diffraction mapping. Appl Phys A Mater Sci Process. 2017;123(484):1–12.
22. Polkownik C, Buisman I. Prussian blue: limitations associated with the analysis of early synthetic pigments and their extenders. Bull Hamilton Kerr Inst. 2020;8:14–27.
23. Kirby J. The painter's trade in the seventeenth century: theory and practice. Natl Gallery Tech Bull. 1999;20.
24. Bristow IC. Interior house-painting colours and technology 1615–1840. New Haven; London: Yale University Press; 1996.
25. Bristow IC. Architectural colour in British interiors 1615–1840. New Haven, CT: Yale University Press; 1996.
26. Dossie R. The handmaid to the arts. 2d edn, wi. London: Printed for J. Nourse; 1764.
27. Merrit C. The art of refining, communicated by Dr. Christopher Merrit. Philos Trans (1665–1678). 1677;12:1046–52.
28. Harris J. Lexicon technicum or, an universal English dictionary of arts and sciences: explaining not only the Terms of Art, but the Arts Themselves. Vol. I. London: Printed for Dan. Browne, Tim. Goodwin, John Walthoe, John Nicholson, Ben. Tooke, Dan. Midwinter, and Tho. Ward; 1716.
29. Boyle R. Certain physiological essays and other tracts (1669): two essays, concerning the unsuccessfulness of experiments. In: Hunter M, Davis EB, editors. The works of Robert Boyle, Vol 2: The Sceptical Chymist and other publications of 1661. 1999.
30. Neri A, Merret C. The art of glass wherein are shown the wayes to make and colour glass, pastes, enamels, lakes, and other curiosities / written in Italian by Antonio Neri; and translated into English, with some observations on the author. Oxford Text Archive (2011); 1662.
31. Howard H. Pigments of English medieval wall painting. Pigments of English medieval wall painting. London: Archetype; 2003.
32. Krekel C, Polborn K. Lime blue—a mediaeval pigment for wall paintings? Stud Conserv. 2003;48(3):171–82.
33. Orna MV, Low MJD, Baer NS. Synthetic Blue Pigments: Ninth to Sixteenth Centuries. I. Literature. Stud Conserv. 1980;25(2):53–63.
34. Orna MV, Low MJD, Julian MM. Synthetic blue pigments: Ninth to Sixteenth Centuries. II. "Silver Blue." Stud Conserv. 1985;30(4):155–60.
35. Thompson DV. The materials and techniques of medieval painting. The materials and techniques of medieval painting. Dover. New York: Dover Publications; 1956.
36. Kosec T, Ćurković HO, Legat A. Investigation of the corrosion protection of chemically and electrochemically formed patinas on recent bronze. Electrochim Acta. 2010;56(2):722–31.
37. Hayez V, Segato T, Hubin A, Terryn H. Study of copper nitrate-based patinas. J Raman Spectrosc. 2006;37:1211–20.
38. Crippa M, Bongiorno V, Piccardo P, Carnasciali MM. A characterisation study on modern bronze sculpture: the artistic patinas of Nado Canuti. Stud Conserv. 2019;64(1):16–23.
39. Graedel TE. Copper patinas formed in the atmopshere—II. A qualitative assessment of mechanisms. Corros Sci. 1987;27(7):721–40.
40. Privitera A, Corbascio A, Calcani G, Della Ventura G, Ricci MA, Sodo A. Raman approach to the forensic study of bronze patinas. J Archaeol Sci Rep. 2021;39: 103115.
41. Chelaru JD, Mureşan LM, Barbu L, Kolozsi T, Pînzaru SC, Tamas T. Characterization of the corrosion products formed on Michael the Brave's equestrian statue in urban atmosphere. Mater Today Commun. 2022;31: 103565.
42. Herman RG, Bogdan CE, Kumler PL, Nuszkowski DM. Preparation and characterization of hydroxycarbonate precursors that yield successful alcohol synthesis catalysts. Mater Chem Phys. 1993;35(3–4):233–9.
43. Guru S, Kumar S, Bellamkonda S, Gangavarapu RR. Synthesis of CuTi-LDH supported on g-C3N4 for electrochemical and photoelectrochemical oxygen evolution reactions. Int J Hydrogen Energy. 2021;46(30):16414–30.
44. Liu B. One-dimensional copper hydroxide nitrate nanorods and nanobelts for radiochemical applications. Nanoscale. 2012;4(22):7194–8.
45. Yu Q, Huang H, Chen R, Wang P, Yang H, Gao M, et al. Synthesis of CuO nanowalnuts and nanoribbons from aqueous solution and their catalytic and electrochemical properties. Nanoscale. 2012;4(8):2613–20.
46. Molchan IS, Thompson GE, Skeldon P, Andriessen R. Synthesis of malachite nanoparticles and their evolution during transmission electron microscopy. J Colloid Interface Sci. 2008;323(2):282–5.
47. Goncharova D, Lapin I, Svetlichnyi V. Structure and optical properties of nanoparticles obtained by pulsed laser ablation of copper in gases. J Phys Conf Ser. 2019;1145(1): 012029.
48. Woods TL, Garrels RM. Use of oxidized copper minerals as environmental indicators. Appl Geochem. 1986;1(2):181–7.
49. Stanimirova TS, Dencheva S, Kirov G. Structural interpretation of anion exchange in divalent copper hydroxysalt minerals. Clay Miner. 2013;48(1):21–36.
50. Cardell C, Herrera A, Guerra I, Navas N, Rodríguez Simón L, Elert K. Pigment-size effect on the physico-chemical behavior of azurite-tempera dosimeters upon natural and accelerated photo aging. Dyes Pigm. 2017;141:53–65.
51. Guillou N, Louer DLM. An X-ray and neutron powder diffraction study of a new polymorphic phase of copper hydroxide nitrate. J Solid State Chem. 1994;109(2):307–14.
52. Lafuente B, Downs RT, Yang H, Stone N. The power of databases: the RRUFF project. In: Armbruster T, Danisi RM, editors. Highlights in mineralogical crystallography. Berlin: W. De Gruyter; 2015. p. 1–30.
53. MacTaggart P, MacTaggart A. Pigment ID using polarised light microscopy. 2007. Blue pigments. https://academicprojects.co.uk/blue-pigments/. Accessed 5 Oct 2023.
54. Naumova MM, Pisareva SA. A note on the use of blue and green copper compounds in paintings. Stud Conserv. 1994;39(4):277–83.
55. Naumova MM, Pisareva SA, Nechiporenko GO. Green copper pigments of Old Russian Frescoes. Stud Conserv. 1990;35(2):81–8.
56. Meyn M, Beneke K, Lagaly G, Chemie A, Kiel U. Anion-exchange hydroxy salts. Inorg Chem. 1993;32(2):1209.
57. Biswick T, Jones W, Pacuła A, Serwicka E. Synthesis, characterisation and anion exchange properties of copper, magnesium, zinc and nickel hydroxy nitrates. J Solid State Chem. 2006;179(1):49–55.
58. Melchiorre EB, Criss RE, Rose TP. Oxygen and carbon isotope study of natural and synthetic azurite. Econ Geol. 2000;95(3):621–8.
59. Downs RT, Hall-Wallace M. The American Mineralogist crystal structure database. Am Miner. 2003;88:247–50.
60. Momma K, Izumi F. VESTA 3 for three-dimensional visualization of crystal, volumetric and morphology data. J Appl Crystallogr. 2011;44:1272–6.
61. Lamb HH. Britain's changing climate. Geogr J. 1967;133(4):445–66.
62. Auray S, Eyquem A, Jouneau-Sion F. Climatic conditions and productivity: an impact evaluation in pre-industrial England. Ann Econ Stat. 2016. https://doi.org/10.15609/annaeconstat2009.121-122.261.
63. Coto B, Martos C, Peña JL, Rodríguez R, Pastor G. Effects in the solubility of CaCO3: experimental study and model description. Fluid Phase Equilib. 2012;324:1–7.
64. Lucile F, Cézac P, Contamine F, Serin JP, Houssin D, Arpentinier P. Solubility of carbon dioxide in water and aqueous solution containing sodium hydroxide at temperatures from (293.15 to 393.15) K and pressure up to 5 MPa: experimental measurements. J Chem Eng Data. 2012;57(3):784–9.
65. Preis W, Gamsjäger H. Solid-solute phase equilibria in aqueous solution. XVI. Thermodynamic properties of malachite and azurite—predominance diagrams for the system Cu2+-H2O-CO2. J Chem Thermodyn. 2002;34(5):631–50.

66. Pourbaix M. Electrochemical corrosion and reduction. In: Brown BF, editor. Corrosion and metal artifacts: a dialogue between conservators and archaeologists and corrosion scientists. US Department of Commerce, National Bureau of Standards; 1977.
67. Bucklow S. Housewife chemistry. In: Wrapson L, Rose J, Miller R, Bucklow S, editors. In artists' footsteps: the reconstruction of pigments and paintings. Archetype Publications; 2012.
68. Harley RD. The interpretation of colour names. Burlingt Mag. 1968;110(785):460–1.
69. Archival material: Insured: James Chabot, 21 Gutter Lane, Gold and Silver Refiner, London Metropolitan Archives, City of London CLC/B/192/F/001/MS11936/369/572207, from the Royal and Sun Alliance Insurance Group, Sun Insurance Office Limited
70. Archival material: Insured: John Moore, 17 Silver Street Wood Street Cheapside, Refiner of Metals, Aqua Fortis Maker and Blue Colour Manufacturer, London Metropolitan Archives, City of London CLC/B/192/F/001/MS11936/399/639034, from the Royal and Sun Alliance Insurance Group, Sun Insurance Office Limited

Publisher's Note